A New Method for the Robust Estimation of the Motile Cilia Beating Frequency

Olivier Meste, Frédéric Brau, Alice Guyon

A New Method for the Robust Estimation of the Motile Cilia Beating Frequency

O. MESTE [1], F. BRAU [2], A. GUYON [2]
[1] Lab I3S, CNRS University of Nice-Sophia Antipolis
[2] IPMC, CNRS University of Nice-Sophia Antipolis

***Abstract*—Motile cilia play a major role in fluid circulation in many biological systems such as the oviduct, the airway and the cerebral ventricles and defects in cilia beating lead to pathologies called ciliopathies. The estimation of the cilia beating frequency (CBF) is of great interest to understand how the CBF modulates the liquid fluxes and how CBF is controled by the intra- and/or extra-cellular medium composition of the ciliated cell in a physiological process. Such estimation is almost impossible to be computed on a single cilium because of overlapping patterns. In addition, motion artifacts and camera defaults may hinder or bias the computation of the frequency variations during long lasting experiments. In this paper is provided a methodological development matching the cilia properties. It is first based on a grid removal and a shift compensation. Second, an harmonic model of the observed cilia through image recordings is proposed within a Maximum Likelihood Estimator framework. It is proven that in contrast to classical approaches the best estimation of the frequency is obtained by averaging the squared Fourier transform of individual pixels followed by a particular summation over the frequency, namely the Compressed Spectrum. Illustrative examples show the performances of this robust method compared to classical ones.**

I. Introduction

As mentioned in [1], motile cilia play a crucial role in clearing mucus and debris from the airways under normal conditions, as can be seen in patients with abnormal airway ciliary beating, namely patients with primary ciliary dyskinesia. Because of its presence in third ventricle of the brain cavities, motile cilia also play a role in circulating cerebro-spinal fluid (CSF), where abnormal ciliary beating has recently been linked to hydrocephalus and other developmental cerebral abnormalities. In addition, they are speculated to be a part of the central glucose sensing system [2]. In both case, the circulation and the clearing are performed by the coordination of the beating cilia producing a wave. The coordination involving several cells is still speculative although it is well accepted that cilia on a single cell beat together. Beating properties are usually addressed by the inverse of the duty cycle, namely the Ciliary Beating Frequency (CBF). This frequency is strongly affected by the molecular components of the cells and the submerging fluid, thus contributing to local homeostatic processes. By this way CBF changes may allow the indirect assessment of metabolic variation. It is clear that the more accurate the estimation of this change will be, the more subtle variation of CBF in response to changes of the medium will be measured.

Unfortunately, cilia are densely packed and close together on all naturally occurring ciliated surfaces. Because this density is observed in the three dimensional case, any imaging system will fail in tracking a single cilium. Instead, the recorded image will be a combination of overlapping cilia, eventually beating at slightly different frequencies. Indeed, because of the long duration experiments and the time constant of the CBF changes according to the molecular components variations, the recording conditions are not optimal and makes difficult the CBF estimation. Furthermore, because of the fluid flux generated by the cilia and the perfusion system, the sample being recorded through the image acquisition system is shifted from frame to frame. Lastly, permanent patterns such as the artifacts due to the acquisition system could be recorded during the experiment and hinder a correct image registration.

The listed limitations can be overcome by using adequate processings usually applied in sequence. Anyhow, this could explain with only few papers cope with the difficult estimation of this frequency while it is of great interest in the Biology field. This problem cannot be efficiently approached using image processing tools such as patterns detection and tracking because of the overlapping cilia. However, attempts based on optical flow [3] and correlation methods [4] failed with our specific application and need high quality records or manual interventions. There is a need for a robust CBF estimator that uses all the prior available to describe advantageously the temporal and spatial properties of the cilia. Many approaches are indeed signal processing methods such as the popular Fourier analysis [5] applied on temporal series. Along the same line, the underlying model is not fully exploited according to the cilia properties when considering classical Fourier analysis.

The present report proposes a methodological approach that will cope with all these limitations and lack of adequate models by first removing grid artifacts, as described in section III. In section IV, the compensation of the geometrical sample shift is explained and illustrated. In section V, a full derivation of our approach is provided, including theoretical development and comparison to Fourier based analysis and evaluated on illustrative examples. This work will be ended by a conclusion.

II. Image acquisition

A. Brain slices

All the protocols were carried out in accordance with French standard ethical guidelines for laboratory animals (Agreement N 75-178, 05/16/2000) and were approved by the IPMC care committee. Attention was paid to use only the number of animals requested to generate reproducible results. 12-80 day old male wild type C57BL6 mice were bred in the local animal

facilities and maintained on a 12h dark/light cycle (7am/7pm) with food and water ad libitum. Mice were decapitated and brains were rapidly removed into ice-cold gassed medium (95% O2/5% CO2) containing (in mM): 125 NaCl, 2.5 KCl, 1 MgCl2, 0.4 CaCl2, 1.25 NaH2PO4, 26 NaHCO3 and 25 glucose. Coronal slices of the median part of the hypothalamus (250m), were cut with a HM650V vibratome (Microm, Walldorf, Germany) and placed in a holding chamber at 34C for 30 min. Slices were then transferred into another incubating chamber at room temperature (22-25C) continuously perfused at a rate of 1-2ml.min-1 with Phosphate Bicarbonate Buffer Saline (PBBS), pH 7.4 when bubbled with 95% O2/5% CO2, containing additional CaCl2 (final concentration: 2mM) and used for recordings. Solutions were applied to the slices through the perfusion system.

B. Acquisition Systems

Two types of acquisition system are typically available for CBF studies. In this context, the confocal microscope technology is mostly used for linescan analysis as described in section V. Xt image sequences were acquired using a TCS SP5 Laser Scanning Confocal Microscope (Leica Microsystems, Nanterre, France) [7]. The brain slice was placed on the stage of the DMI6000 inverted microscope and first, a bright field image was done (XY scan) with the 488 nm laser line using the transmission detector (image a), through a HCX APO 40X/0.80 Water immersion objective. Then a line was drawn perpendicular to the axis of the cilia and a scanning was done in Xt mode along this line with a sampling frequency of 1400 Hz . Synthetic images (512x1024 pixels corresponding to a duration of 0.73 sec) of the traces of the beating of the cilia were recorded each 10 sec during the experiment.

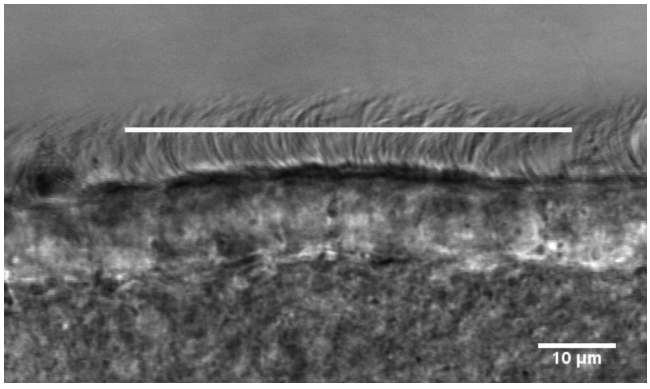

Fig. 1. A line is drawn parallel to the surface of the ciliate cells where the cilia are moving. The light intensity is determined along this line and plotted against time to build a synthetic image.

The second system acquires bright field image sequences on an upright Axioskop microscope (CarlZeiss, Le Pecq, France) using an ApoChromat 63X/1 water immersion objective. 200 images were captured every minute at a frame rate of 200 frames/ second with a GigE Vision color CMOS camera (PicSight, Leutron Vision, Switzerland). To use the camera at its maximum speed, the image size was reduced to acquire a 200x200 pixels sub area of the image. The acquisition and

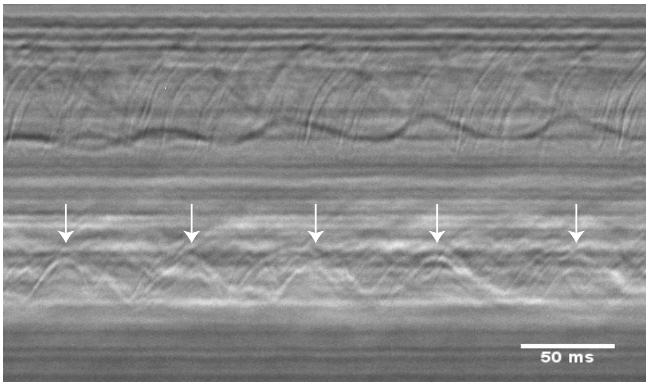

Fig. 2. Synthetic Xt image obtained by scanning along a line perpendicular to the axis of the cilia. The CBF is determined by the average of the period calculated on 5 peaks of the sinusoids obtained in the plot of light intensity against time.

automatic recording of all the successive 1sec sequences was done using StreamPix software (Norpix, Montreal, Canada). This second acquisition system was prefered to be used in routine analysis in place of the confocal linescan [8] strategy more sensitive to the focus drifts and the movements of the sample. However, the image recorded through this second system will be also processed offline with a linescan analysis similar to the one used with confocal microscope, for comparison.

III. Artifacts removal

Grid pattern in the CCD sensor is one artifact that should be removed prior to any image processing. The image frame from the second acquisition system displayed in fig. 3 and the averaged image AV from a sequence of 200 images displayed in fig. 4 clearly exhibit such frame in addition to the cilia. Note that while the cilia don't appear in the average image because of the moving pattern, the grid is still visible because of its permanent location. We consider now the acquisition of a background sequence of 200 images (same illumination, without brain slice) and its computed average AVG displayed in fig. 5

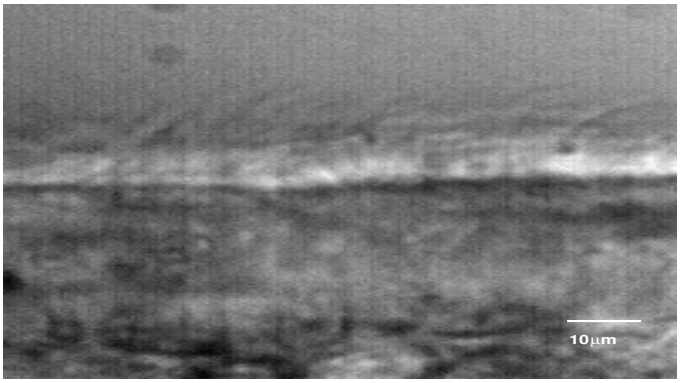

Fig. 3. A single frame containing ciliary beating and interferences

It is assumed now that the grid AVG is added to each frame, and consequently to the average image AV, up to a constant multiplicative factor. This factor remains to be estimated in

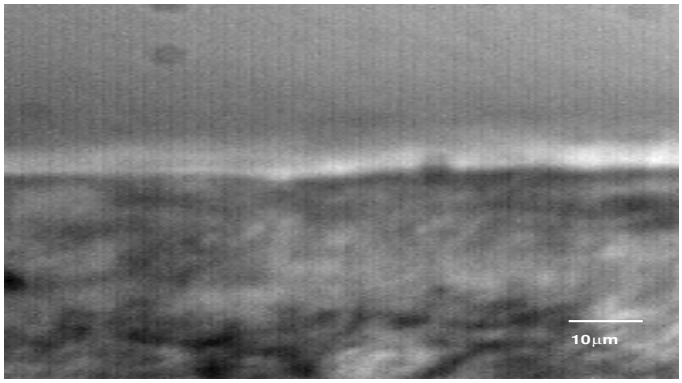

Fig. 4. Averaged frames AV containing ciliary beating and interferences

order to efficiently subtract the grid. A single line of the frames is considered to compute this estimation. Let's call $av(n)$ and $avg(n)$ the corresponding lines of AV and AVG, whose means have been subtracted and where n stands for the column index. Lines that are free of cilia samples will produce better estimation. Considering the illustrative examples of fig. 4 and fig. 5, a line parallel to the border of the sample will be selected for the following computation.

The statistical properties of the line $av(n)$ do not allow an efficient use of a least square method for the estimation. Indeed, with respect to the periodical spatial properties of the grid, it can be proven that the autocorrelation function of $avg(n)$ exhibits a large spike for lag $m = 0$, i.e. column shift equal 0. Thus, for a guessed value α of the multiplicative coefficient that has to be estimated, the correlation function is computed such as:

$$r(m,\alpha) = \sum_{n=0}^{N-m-1} \left[av(n) - \alpha.avg(n)\right] avg(n+m) \qquad (1)$$

where N stands for the length of the two lines.

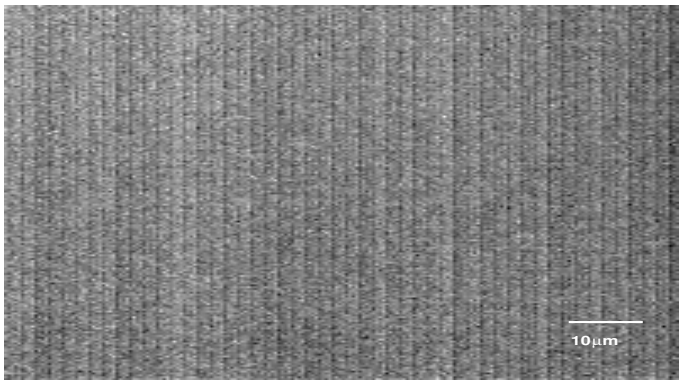

Fig. 5. Average of frames (from a blank field) AVG containing only interferences

An example of $r(m,0)$ is displayed in fig. 6, where the spike at $m = 0$ is clearly visible.

In order to estimate the correct value of the coefficient we propose to use an exhaustive search of the minimum value of

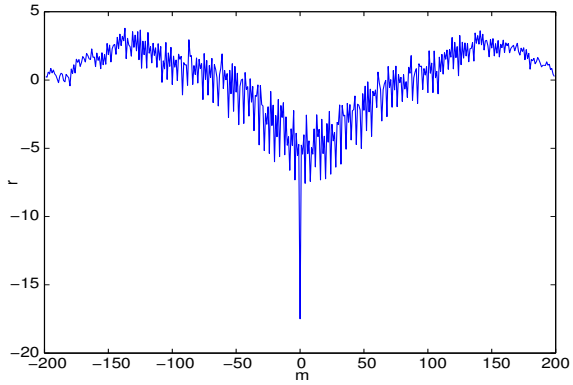

Fig. 6. The correlation function $r(m,\alpha)$ for the value $\alpha = 0$

the criteria:

$$c(\alpha) = \frac{|r(0,\alpha) - r(1,\alpha)| + |r(0,\alpha) - r(-1,\alpha)|}{|r(1,\alpha)| + |r(-1,\alpha)|} \qquad (2)$$

with respect to the parameter α. This criteria tends to be high as long as the grid remains in the line of interest, and small when the grid is perfectly removed. This criteria is given in fig. 7 where a minimum is visible for the value $\alpha = 0.55$.

The corresponding function $r(m, 0.55)$ is displayed in fig. 8, where compared to fig. 6 the spike has been perfectly substracted, meaning that the introduced criteria is adequate and the coefficient accurately estimated.

Once the coefficient has been estimated, the weighted average image AVG containing the grid can be subtracted to the average image that contains the beating cilia. The figure fig. 9 shows that compared to the contaminated one (see fig. 4) the grid has been perfectly removed. This corrected average image will be used in the following as the reference for the registration process that will allow the image realignment.

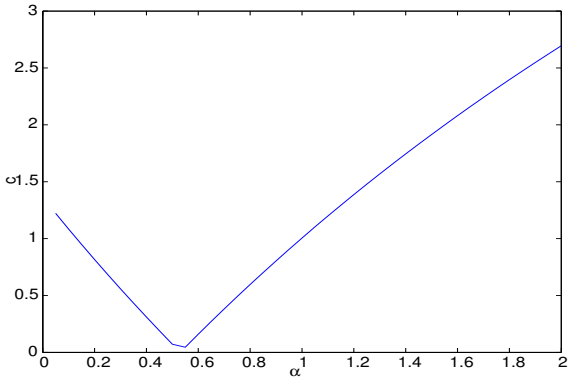

Fig. 7. The criteria $c(\alpha)$ with a clear minimum

IV. Image registration process

Once the grid and the background are removed from the reference image (called RIM) and from each frame, the spatial shift due to the moving effect of the sample has to be estimated. It is worth noting that this loss of alignment leads to an error in the frequency computation. For each frame IM_k,

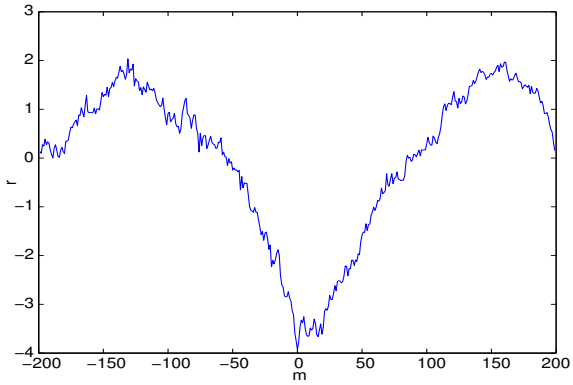

Fig. 8. The correlation function $r(m, \alpha)$ with the correct coefficient value $\alpha = 0.55$

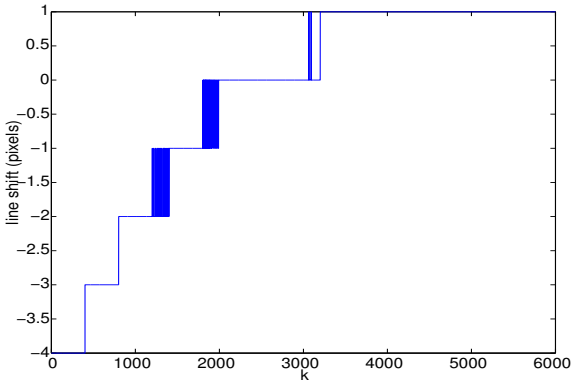

Fig. 10. The estimated line shift (pixels) for each frame ($k = 1 \ldots 6000$)

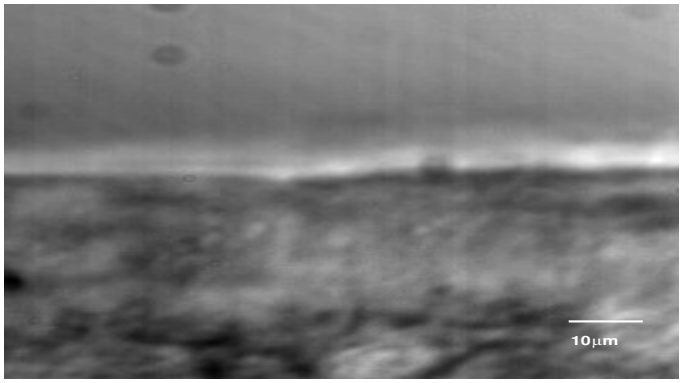

Fig. 9. Average of frames where the interferences have been removed

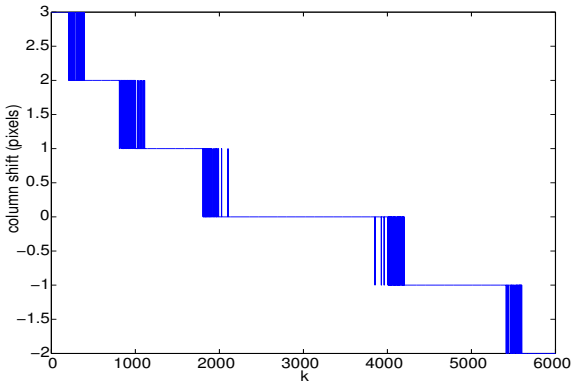

Fig. 11. The estimated column shift (pixels) for each frame ($k = 1 \ldots 6000$)

the optimal two-dimensional $(\hat{li}, \hat{co})$ alignment or registration is estimated by using the minimization:

$$(\hat{li}, \hat{co}) = \arg\min_{li,col} \sum_i \sum_j (IM_k(i,j) - RIM(i+li, j+col))^2 \quad (3)$$

An exhaustive search is computed within a range of possible values using the full images. This criteria, similar to a cross-correlation function, produces for each image IM_k a pair of values that will allow the alignment of the frames sequence. In [9], in addition to the optimal estimation of the reference image an iterative scheme is proposed for realignment in the one dimensional case that could be easily extended to this application. However, an exhaustive search guarantees to reach the optimal values and can be speeded up by reducing the search domain according to the alignment data estimated from the previous image. Indeed, because of the low strength exerted by the cilia and the slow perfusion flow, the spatial shift observed frame by frame is weak allowing an efficient relative realignment. An example of the registration performed of a sequence of 6000 frames is given in figure 10,11 where it can be noticed that the shift is weak and continuous along the acquisition. In fig.12, it is clear that the spatial shift is almost diagonal in this experiment.

Note that optimality of the estimation is not addressed in this study. However, because it is based on mean square minimization, asymptotically optimal when the noise is gaussian, the estimation will be robust with respect to interferences. To this respect, the image alignment is indeed influenced by the static part of the sample and not by the cilia. It means that the registration will not track the cilia motion because it plays a very little role in the global image variation considered frame by frame. Furthermore, the complex nature of the cilia observation, including overlapping and multiplicity, does not allow a direct tracking frame by frame of a single cilium. In spite of these limitations, a global modeling of the sub image containing only cilia will be proposed as shown in the following

V. Frequency Estimation

Two classic measurements of the Cilia Beating Frequency (CBF) consist in a visual inspection of concatenated lines, named confocal linescan and the computation of the Fast Fourier Transform (FFT) of averaged pixels. These two methods will be briefly introduced, followed by the development of a new method named MLE.

A. Confocal Linescan

From the first system described in section II a synthetic image (fig. 2) is created where the periodic behavior of the cilia pattern should be visible. The peaks of the sinusoids were manually determined for each file (arrows in fig. 2) and the frequency was calculated from the average of 5-6 in between

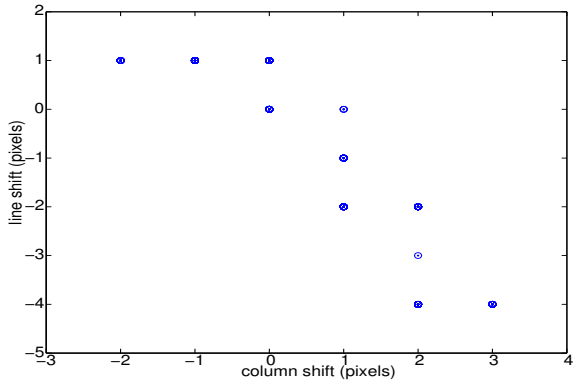

Fig. 12. The estimated pairs of spatial shifts (pixels). They are mostly superimposed because of the small variations estimated as integers

peak measurements using an homemade ImageJ (Wayne Rasband, National Institute of Mental Health, Bethesda, Maryland, USA) macro. In addition to demanding acquisition conditions, this computation needs manual interventions leading to a large variance in the CBF estimation.

B. Average of pixel intensity

As the name implies, first the pixel intensities in the entire sub-image was averaged. This averaged value gave the average pixel intensity of the sub-image. This process was done for the entire set of images. The Fast Fourier Transform (FFT) of the average value was then obtained. We plotted the frequency vs. magnitude, the frequency with the maximum magnitude giving the CBF. This method was rather simple and not much computationally costly.

C. Average of the FFT of individual pixels

Here first the squared modulus of FFT of the individual pixels of the sub image were obtained. Once this process was completed, they were stored. This process repeats for all the pixels in all the sub images in the given set of images. Then, the average of the processed FFT is obtained and plotted. Thus a plot of frequency vs. magnitude is obtained. The frequency with the maximum magnitude is the CBF. This second method was much more computationally costly but quite effective. Note that in contrast to the average of pixels, the modulus of the FFT is invariant with respect to delay in the time domain. It is expected that due to its own motion, one cilia affects pixels in a bounded area with a small delay function of the velocity and the inter-pixel distance. This fact is in favor of any spectral approach based on modulus averaging.

Although the behavior model definition of single cilia may be well addressed [6], the estimation of the CBF based on this model is a difficult task due to the observation itself. This difficulty is explained not only by the presence of artifacts such as acquisition noise and spatial shift of the active ciliated cells but also because of the overlapping multiple cilia. This phenomenon makes tedious the frame by frame tracking of geometrical features and consequently hinders the accurate estimation of the CBF. In contrast to this spatial approach, robustness and accuracy are improved by considering temporal and spatial coherence. In other words, we consider that within a region of interest, all pixels share a common temporal feature, maybe shifted in time, that is the frame by frame intensity variation. Eventually, pixels could also capture adjacent cilia beating at the same frequency because of the metachronal waves. Assuming that the variation is periodical and that each pixel records an abrupt intensity variation, we propose a harmonic model that combines the fundamental frequency (f) and the first and second harmonics. Considering that the model should be invariant with respect to time delays, each pixel intensity variation $p_i(t)$ from the total I within the sub-image, is modeled by:

$$p_i(t) = \sum_{j=1}^{3} [\theta_{i,2j-1} cos(2\pi f j t) + \theta_{i,2j} sin(2\pi f j t)] + n_i(t) \quad (4)$$

Where $n_i(t)$ is a white gaussian error composed by the modeling error and observation noise. In this model, j and θ stand for the harmonic number and weight of the decomposition, respectively. Its is worth noticing that pairs of values $(\theta_{i,2j-1}, \theta_{i,2j})$ convey information of both the amplitude of the harmonic and its temporal shift although the analysis is focused on the frequency (f). Among the available estimators provided by the estimation theory, the Maximum Likelihood Estimator (MLE) [10] is selected for its properties with respect to the error. It is assumed here that the error is gaussian, stationary and uncorrelated spatially and temporally. Considering the I pixels from the sub-image, maximizing the likelihood function is equivalent to minimize the following criteria:

$$J_1 = \sum_{i=1}^{I} \|\mathbf{p}_i - M_f \boldsymbol{\theta}_i\|^2 \quad (5)$$

Where $\mathbf{p}_i$ and $\boldsymbol{\theta}_i$ stand for the vector formed by the temporal values of pixel i extracted from the successive frames and the parameters vector, respectively. Note that temporal delays introduced by the sequential recording of the motile cilia by adjacent pixels are inherent to the model. In this model, the parameter f is the fundamental frequency and only the first and second harmonics are taken into account. Then, M_f matrix contains cosines and sines functions defined over the time t_k (with $t_1 \leqslant t_k \leqslant t_K$) corresponding to the acquisition of the frames such that:

$$M_f = [M_{1.f} \;\; M_{2.f} \;\; M_{3.f}] \quad (6)$$

with

$$M_{j.f} \;\; = \;\; \begin{pmatrix} cos(2\pi f j t_1) & sin(2\pi f j t_1) \\ \vdots & \vdots \\ cos(2\pi f j t_K) & sin(2\pi f j t_K) \end{pmatrix}$$

Indeed, the criteria J_1 has to be minimized with respect to the set of parameters f and $\boldsymbol{\theta}_i$'s. Developing (5), the solution is thus given by the minimization:

$$\left(\hat{\boldsymbol{\theta}}_1, \ldots, \hat{\boldsymbol{\theta}}_I, \hat{f}\right)$$

$$= \arg \min_{\boldsymbol{\theta}_1, \ldots, \boldsymbol{\theta}_I, f} \sum_{i=1}^{I} \left[\mathbf{p}_i^T \mathbf{p}_i - 2\mathbf{p}_i^T M_f \boldsymbol{\theta}_i + \boldsymbol{\theta}_i^T M_f^T M_f \boldsymbol{\theta}_i\right] \quad (7)$$

The derivation of the criteria with respect to the vectors $\boldsymbol{\theta}_i$ provides the estimated $\hat{\boldsymbol{\theta}}_i$'s:

$$\begin{aligned}\hat{\boldsymbol{\theta}}_i &= [\hat{\theta}_{i,1}, \hat{\theta}_{i,2}, \hat{\theta}_{i,3}, \hat{\theta}_{i,4}, \hat{\theta}_{i,5}, \hat{\theta}_{i,6}]^T \\ &= (M_f^T M_f)^{-1} M_f^T \mathbf{p}_i \end{aligned} \quad (8)$$

It can be proven that after substituting these solutions in (7), the minimization is finally a maximization with respect to f:

$$\hat{f} = \arg\max_f \sum_{i=1}^{I} \mathbf{p}_i^T M_f (M_f^T M_f)^{-1} M_f^T \mathbf{p}_i \quad (9)$$

Whatever the value of f, the matrix $(M_f^T M_f)^{-1}$ can be approximated by kI, where I stand for the identity matrix and k a constant. Note that for specific values of f this approximation is indeed the equality. Thus (8) is simplified by:

$$\hat{\boldsymbol{\theta}}_i = k M_f^T \mathbf{p}_i \quad (10)$$

and (9) can be replaced by:

$$\hat{f} = \arg\max_f \sum_{i=1}^{I} \hat{\boldsymbol{\theta}}_i^T \hat{\boldsymbol{\theta}}_i \quad (11)$$

In fact, a sum $(\hat{\theta}_{i,2j-1}^2 + \hat{\theta}_{i,2j}^2)$ with $j = 1, 2, 3$ is equivalent to the squared modulus of the Fourier Transform (FT) at the frequency $j.f$, namely $|FT(\mathbf{p}_i)|^2(j.f)$. Thus the maximization in (9) is equivalent to:

$$\hat{f} = \arg\max_f \sum_{j=1}^{3} \sum_{i=1}^{I} |FT(\mathbf{p}_i)|^2(j.f) \quad (12)$$

The sum of the squared modulus of the fundamental frequency and its harmonics is also called the Compressed Spectrum $CS(f)$. Then, (12) is replaced by:

$$\hat{f} = \arg\max_f \sum_{i=1}^{I} CS_i(f) \quad (13)$$

This last expression allows an easy interpretation of this maximization, using the mentioned approximation. It is finally equivalent to the problem addressed by the average of squared modulus of FFT where the harmonic modeling is accounted in the estimation. In summary, this last solution uses all the priors related to the observation of the motile cilia. Note that the optimization (12) should be performed over the single parameter f. Sophisticated optimization algorithms are available but with the risk of converging toward a local maxima. We will prefer in the sequel an exhaustive search over a given range of the f values, allowing the addition of a priori knowledge and fixing the frequency resolution.

D. Methods evaluation

Albeit the linescan technique has been designed to work on image captured by confocal microscope it has been tested on the second acquisition system because it will be preferred for routine acquisition.

In fig. 13 is given the linescan image from this system where the extraction of the periodic pattern seems to be feasible (see white arrows), however confounding. Nevertheless, such method fails in providing accurate CBF estimates with such image. Instead, the following methods will be preferred for their good performances with such image acquisition modality.

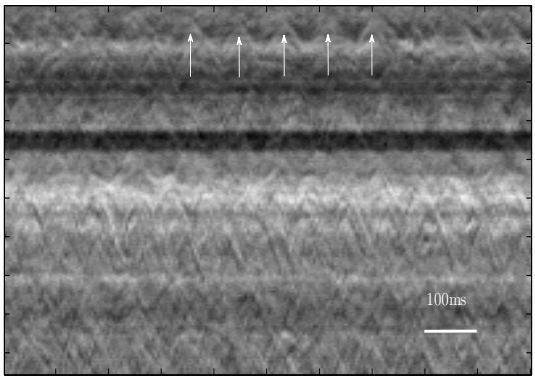

Fig. 13. Synthetic image built with the same method than for the linescan, applied to bright field images. The light intensity is determined along a line and plotted against time

In order to focus the analysis on a small set of cilia's, it is defined a 3x17 pixels sub image in the vicinity of the cilia base (black rectangles in fig. 14).

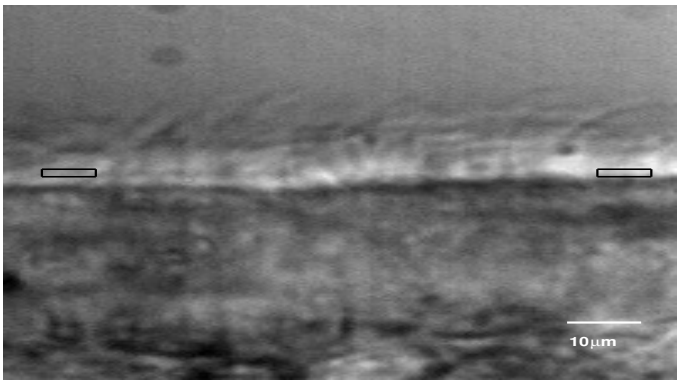

Fig. 14. Left and right sub images bounded by black rectangles defining regions of interest

Each pixel p_i in the sub image will define a vector when considering its intensity frame by frame. A sequence of 200 frames corresponding to 1 second (the time is sampled with a frequency equal to $\approx$ 200Hz) is analyzed by using the three approach: squared modulus of the FFT of the average pixel, average of the squared modulus of the FFT for each individual pixel, Maximum Likelihood Estimator. An illustrative example of such processing is provided in fig. 15 and fig. 16, by using the right sub image in fig. 14. It is clear in fig. 15 that the FFT of averaged pixel contains less harmonics of the fundamental frequency in contrast to the averaged FFT. This loss of information could be explained by the averaging process when considering delayed signals. In fig. 16, the function to be minimized is computed over the expected frequencies interval [8-30]Hz allowing to limit the search domain of the minimization. For the three methods the estimated CBF is

about 11Hz.

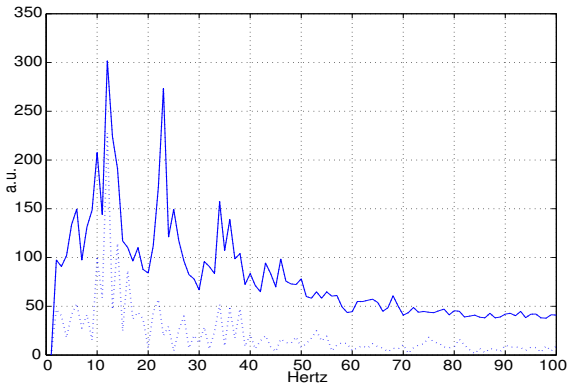

Fig. 15. Average of squared FFT (solid line), squared FFT of averaged pixels (dotted line)

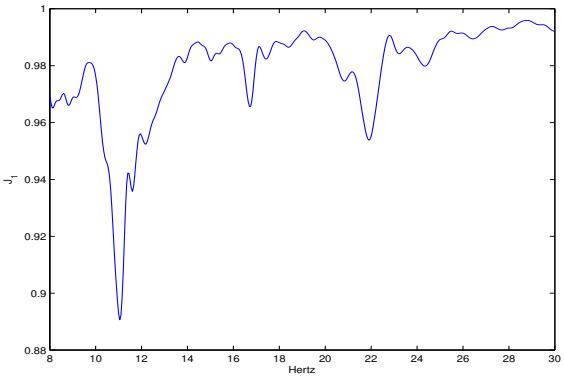

Fig. 16. The MLE criteria J_1 function of the frequency

In order to analyze the time-varying CBF, sequences of 200 frames are processed every 10 seconds. So, for a total amount of 6000 frames, 30 estimated CBF are provided by the mentioned methods for two sub images (in fig. 14, left and right rectangles). In fig. 17 and fig. 18, the results from the averaged FFT, FFT of averaged pixels, MLE are given for the two sub images, respectively. It can be noticed that results are almost similar whatever the sub images and the method. However, the MLE methods slightly outperforms the others because the frequency variations tends to be smoother, as what is expected.

VI. Conclusion

Motivated by the great interest in the Biology field for CBF measurement, an estimator has been proposed according to the priors available in the time and spatial domain. Robustness has been addressed by introducing a harmonic model of the temporal variations of pixels intensities. It is worth noting that amplitudes and frequencies have been assumed constant in the sequences of 200 frames. A more general extended model could be introduced to overcome this limitation but with the counterpart of a lower robustness and a higher computational cost.

It has been shown that the resulting method has a clear interpretation in term of time-invariant estimation. In parallel with an image artifacts removal, the method outputs exhibit lower variability as expected.

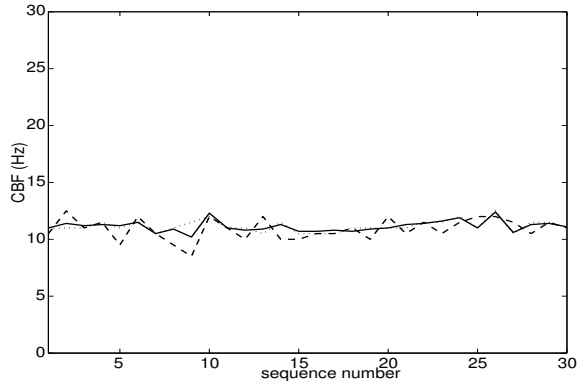

Fig. 17. CBF within the right sub image: averaged FFT (dotted line), FFT of averaged pixels (dashed line), MLE (solid line)

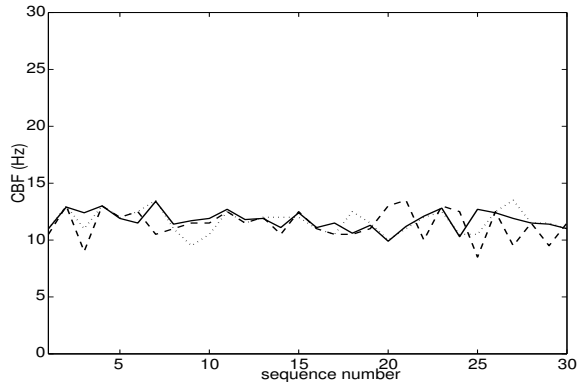

Fig. 18. CBF within the left sub image: averaged FFT (dotted line), FFT of averaged pixels (dashed line), MLE (solid line)

Acknowledgement

Authors would like to thank N. Ramkumar, G. Conductier and J.L. Nahon for their contributions to this work. This work has been partly funded by grant PEPS 2010 and supported by INSB.

References

[1] Salathe M. Regulation of mammalian ciliary beating. Annu Rev Physiol 2007; 69:401-422.
[2] Garcia MA, et al. Hypothalamic ependymal-glial cells express the glucose transporter GLUT2, a protein involved in glucose sensing. J Neurochem 2003; 86:709-724.
[3] Kim W, Han TH, Kim HJ, Park MY, Kim KS, Park RW. An Automated Measurement of Ciliary Beating Frequency using a Combined Optical Flow and Peak Detection. Health Inform Res. 2011 Jun;17(2):111-9.
[4] Yi WJ, Park KS, Lee CH, Rhee CS, Nam SW. Directional disorder of ciliary metachronal waves using two-dimensional correlation map. IEEE Trans Biomed Eng. 2002 Mar;49(3):269-73.
[5] Yi WJ, Park KS, Lee CH, Rhee CS. Correlation between ciliary beat frequency and metachronal wave disorder using image analysis method. Med Biol Eng Comput. 2003 Jul;41(4):481-5.
[6] O'Callaghan C, et al. Analysis of ependymal ciliary beat pattern and beat frequency using high speed imaging: comparison with the photo-multiplier and photodiode methods. Cilia, 2012, 1:8
[7] Doyle RT, Moninger T, Debavalya N, Hsu WH. Use of confocal linescan to document ciliary beat frequency. J Microsc. 2006 Aug;223(Pt 2):159-64.

[8] Lechtrek KF, Sanderson MJ, Witman GB. High-speed digital imaging of ependymal cilia in the murine brain. Methods in Cell Biol, 2009, (91):255-264.
[9] Cabasson A, Meste O. Time Delay Estimation: A New Insight Into the Woody's Method, IEEE Signal Processing Letters 2008, 15: 573-576.
[10] Kay SM. Fundamentals of StatisticalSignal Processing. Ed. Prentice Hall, 1993.
[11] Del Bigio MR. Ependymal cells: biology and pathology. Acta Neuropathol 2010; 119:55-73.
[12] Psarra AM, et al. Immunocytochemical localization of glycogen phosphorylase kinase in rat brain sections and in glial and neuronal primary cultures. J Neurocytol 1998; 27:779-790.
[13] Teff Z, Priel Z, Gheber LA. The forces applied by cilia depend linearly on their frequency due to constant geometry of the effective stroke. Biophys J 2008; 94:298-305.